HHS Public Access

Author manuscript

Cancer Cell. Author manuscript; available in PMC 2017 December 12.

Published in final edited form as:

Cancer Cell. 2016 December 12; 30(6): 940–952. doi:10.1016/j.ccell.2016.11.006.

Leveraging an NQO1 Bioactivatable Drug for Tumor-Selective Use of Poly(ADP-ribose) Polymerase (PARP) Inhibitors

Xiumei Huang[1], **Edward A. Motea**[1], **Zachary R. Moore**[1], **Jun Yao**[1], **Ying Dong**[1], **Gaurab Chakrabarti**[1], **Jessica A. Kilgore**[2], **Molly A. Silvers**[1], **Praveen L. Patidar**[1], **Agnieszka Cholka**[1], **Farjana Fattah**[1], **Yoonjeong Cha**[3], **Glenda G. Anderson**[4], **Rebecca Kusko**[3], **Michael Peyton**[5], **Jingsheng Yan**[6], **Xian-Jin Xie**[6], **Venetia Sarode**[7], **Noelle S. Williams**[2], **John D. Minna**[5], **Muhammad Beg**[5], **David E. Gerber**[5], **Erik A. Bey**[8,#], and **David A. Boothman**[1,#]

[1]Departments of Pharmacology and Radiation Oncology, Simmons Comprehensive Cancer Center (SCCC), UT Southwestern Medical Center (UTSW), Dallas, TX 75390 USA

[2]Department of Biochemistry, SCCC, UTSW, Dallas, TX 75390 USA

[3]Immuneering Corporation, One Broadway 14th Floor, Cambridge, MA 02142 USA

[4]5Degrees Bio., Inc., 111 N. Market Street #300 San Jose, CA 95113 USA

[5]Department of Internal Medicine, Division of Hematology-Oncology, UTSW, Dallas, TX 75390 USA

[6]Department of Biostatistics, UTSW, Dallas, TX 75390 USA

[7]Department of Pathology, UTSW, Dallas, TX 75390 USA

[8]Department of Pharmaceutical Sciences, West Virginia University Health Sciences Center, Morgantown, WV 26508 USA

Summary

Therapeutic drugs that block DNA repair, including poly(ADP-ribose) polymerase (PARP) inhibitors, fail due to lack of tumor-selectivity. When PARP inhibitors and β-lapachone are combined, synergistic antitumor activity results from sustained NAD(P)H levels that refuel NQO1-dependent futile redox drug recycling. Significant oxygen consumption rate/reactive oxygen species cause dramatic DNA lesion increases that are not repaired due to PARP inhibition. In *NQO1*$^{+}$ cancers, such as non-small cell lung, pancreatic and breast, cell death mechanism switches from PARP1 hyperactivation-mediated programmed necrosis with β-lapachone monotherapy to synergistic tumor-selective, caspase-dependent apoptosis with PARP inhibitors and β-lapachone.

[#]Correspondence: Erik.Bey@hsc.wvu.edu or David.Boothman@UTSouthwestern.edu (lead).

Author contributions

Concepts and designs: XH, EAB, DAB; Methodology: XH, EAM, ZRM, JY, YD, GC, JAK, MAS, PLP, AC, FF, YC, MP, JY; Data acquisition: XH, GGA, RK, JX, VS, NSW, EAB, EAM; Analytics: XH, EAM, ZRM, GC, GGA, RK, JX, VS, NSW, JDM, DEG, MB, EAB, DAB; Administrative: JDM, MB, DEG, EAB, NSW, DAB; Writing: XH, ZRM, NSW, DEG, EAM, DAB; Supervision: XH, EAB, DAB.

Synergistic antitumor efficacy and prolonged survival were noted in human orthotopic pancreatic and non-small cell lung xenograft models, expanding use and efficacy of PARP inhibitors for human cancer therapy.

Graphical Abstract

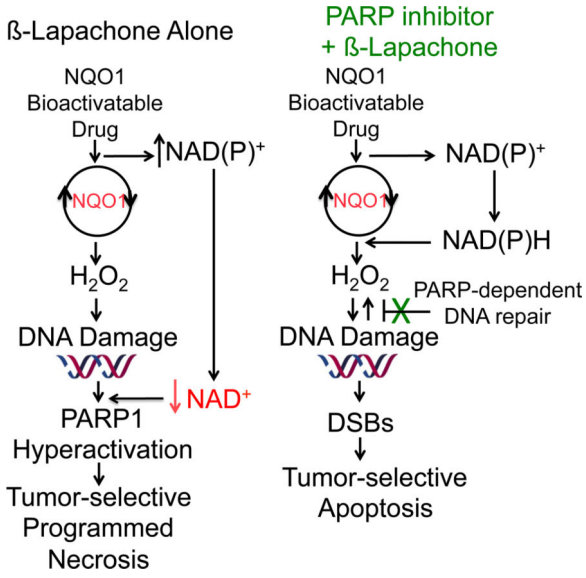

Introduction

Poly(ADP-ribose) polymerase-1 (PARP1) is crucial to multiple DNA repair pathways, including DNA base excision (BER), single strand (SSB) and double strand break (DSB) repair (Dantzer et al., 2000; Wang et al., 2006). Once bound to DNA lesions, PARP1 consumes NAD^+ and PARylates nearby proteins, with activation and deactivation consequences. Self-PARylation (PAR-PARP1) is a post-translational modification that enzymatically inactivates the protein, rendering it unable to bind DNA and function in DNA repair (Helleday et al., 2008; Lee et al., 2014). DNA repair defects in breast cancer associated genes 1 and 2 (BRCA1/2) yielded hypersensitivity to PARP inhibition and caused a rush to develop new PARP inhibitors for targeted therapy in these rare (~5%) hereditary breast and ovarian cancers (Farmer et al., 2005; Sandhu et al., 2013; Underhill et al., 2011). This subtype of cancers exhibits defective homologous recombination (HR) repair and reliance on PARP-dependent alternative non-homologous end joining (Alt-NHEJ) for survival. Exposing HR-defective BRCA1/2 cells to PARP inhibitors results in synthetic lethality that stimulated great interest in PARP inhibitors (Farmer et al., 2005). Attempts to broaden their clinical application, including combined approaches using DNA damaging agents (e.g., ionizing radiation (IR), temozolomide, or gemcitabine (Albert et al., 2007; Jacob et al., 2007; Rajan et al., 2012)) limited tumor-selective rationale and increased normal tissue toxicities.

NAD(P)H:quinone oxidoreductase 1 (*NQO1*) bioactivatable drugs have the potential to deliver tumor-selective DNA damage and cell death. They are a unique class of rare

quinones that include β-lapachone (β-lap, ARQ761 in clinical form) and deoxynyboquinone (Huang et al., 2012). NQO1 catalyzes the two-electron oxidoreduction of β-lap to generate an unstable hydroquinone that spontaneously reacts in a two-step back-reaction with oxygen to regenerate the original compound (Bey et al., 2007). NQO1-dependent futile redox cycling oxidizes ~60 moles of NAD(P)H to create ~120 moles of reactive oxygen species (ROS) in ~2 min (Pink et al., 2000). High levels of superoxide dismutase (SOD) in cancers generate long-lived and cell membrane-permeable hydrogen peroxide (H_2O_2) that diffuses into nuclei to induce massive oxidative base and SSB DNA lesions. A significant bystander effect, blocked by Catalase (*CAT*), occurs from *NQO1*$^+$ cancer cells affecting neighboring *NQO1*$^-$ cancer cells (Bey et al., 2007; Cao et al., 2014). Rapid accumulation of DNA lesions overwhelms DNA repair capacity and causes 'hyperactivation' of PARP. Rapid protein PARylation, including PAR-PARP1, severe NAD^+/ATP depletion, massive DNA lesions and repair inhibition follows (Huang et al., 2012). ROS (H_2O_2) formation only occurs while pools of NAD(P)H are available for NQO1-driven futile redox cycling. A lethal β-lap dose induces caspase-independent programmed necrosis (i.e., NAD^+-Keresis) (Moore et al., 2015). β-Lap-induced cell death is specific for cancers over-expressing NQO1 and suppresses GAPDH/glycolysis, OXPHOS, triggering μ-calpain-directed programmed necrosis (Bey et al., 2007; Pink et al., 2000; Tagliarino et al., 2001). Although β-lap shows evidence of single-agent activity in phase 1 clinical trials, strategies to enhance its efficacy without augmenting toxicity are needed (Gerber et al., 2007). We hypothesized that inhibiting PARP activity prior to β-lap exposure would enhance both agents, extending NQO1-medialed ROS production and inhibiting PARP-driven DNA repair in a tumor-selective manner.

Results

NQO1:CAT ratios offer an exploitable therapeutic window

Examination of *NQO1* (Figure 1A) and *CAT* (Figure 1B) mRNA expression in matched NSCLC tumor tissue showed relatively elevated *NQO1* expression, with concomitant lowered *CAT* levels vs associated normal tissue. As reported (Bey et al., 2007; Siegel et al., 1998), a significant ($p \leq 2.2 \times 10^{-38}$) elevation in *NQO1* mRNA levels in a larger dataset (n=432) of NSCLC patient tumor vs associated normal lung tissue by gene expression microarray analyses was noted (Figure 1C). In contrast, *CAT* mRNA expression was significantly lower ($p \leq 5.6 \times 10^{-48}$) in tumor vs normal lung tissue (Figure 1D). Concomitant high *NQO1* and low *CAT* mRNA levels (high *NQO1:CAT* ratios ($p \leq 1.1 \times 10^{-88}$), Figure 1E) in NSCLC tumor tissue offer an ideal target for NQO1 bioactivatable drugs. Fresh, snapfrozen pathology-assisted dissection of tumor vs associated normal tissue from NSCLC patients confirmed elevated NQO1 enzyme levels in tumor vs normal tissue (Figure 1F). Western analyses confirmed lowered *CAT* levels in NSCLC tumors, with high levels in associated normal lung tissue (Figure 1G). Immunohistochemical (IHC) analyses confirmed NQO1 elevations in NSCLC, PDA and high grade cancers, including triple-negative breast cancers (TNBCs) (Figure S1A). Enzyme assays confirmed elevated NQO1 levels in cancer vs associated normal tissue (Figure S1B, S1C), even when protein was not noted by Westerns (patient 2823, Figure 1G). Advanced and treatment-resistant NSCLC cases also exhibit *NQO1* over-expression, with increased levels in progressive disease (PD)

vs patients who exhibited clinical responses (CR) (Figure S1D). Elevated *NQO1* levels were greater in high vs low grade PDAs (Figure S1E).

β-Lapachone lethality is NQO1-dependent, but not influenced by oncogenic driver or passenger mutations

A >50-member NSCLC cell line panel was used to examine the roles of NQO1 and oncogenic driver and passenger mutations in lethality by β-lap. LD_{50} values for each NSCLC cell line were determined, with or without β-lap (μM, 2 hr) treatment, ± dicoumarol, a fairly specific NQO1 inhibitor (not shown). In a double-blind manner, NQO1 enzyme levels and polymorphism status (i.e., *2 (C609T) or *3 (C465T)) assessments via restriction fragment length polymorphism (RFLP) analyses were measured (Figure 2). LD_{50} values for β-lap-treated NSCLC cell lines ranged between 1–4 μM, 2 hr, regardless of oncogenic or passenger mutations or deletions. At least one wild-type *NQO1* allele was sufficient for efficient cell killing by β-lap, as heterozygous *2 or *3 *NQO1* single nucleotide polymorphism (SNP) cells were killed with equal efficacy as homozygous wild-type cancer cells. Inhibition of NQO1 by dicoumarol (50 μM, 2 hr) spared β-lap lethality (not shown), with LD_{50} values of >20 μM, the highest concentrations used. In contrast, NSCLC cells with homozygous *NQO1* polymorphic alleles (i.e., *2 or *3) that lack NQO1 activities (Bey et al., 2007; Bey et al., 2013) were resistant. Similar hypersensitivities of PDA and breast cancer cells to β-lap (2–6 μM, 2 hr), independent of KRAS, p53, or other oncogenic driver and/or passenger mutations were also noted (Figure S2A, S2B). Lethality caused by β-lap in *NQO1*$^+$ cancer cell lines was noted in all subtypes, as seen in prostate cancer (Planchon et al., 2001). Dicoumarol (DIC, 50 μM, 2 hr) spared *NQO1*$^+$ cancer cell lines, while inherently resistant *NQO1* polymorphic cells were not sensitive. Re-expression of wild-type NQO1 in several PDA or breast *NQO1* polymorphic cancer cells restored sensitivity to β-lap at the 2–6 μM LD_{50} range, and dicoumarol spared lethality (Figure S2A, S2B). A similar screen of NSCLC cell lines exposed to docetaxel or pemetrexed revealed wide-ranging LD_{50} values with no recognizable sensitivity or resistance relationships with mutations (Figure S2C, S2D).

PARP inhibitors synergize with sublethal doses of β-lapachone in an NQO1-dependent manner

We theorized that inhibiting PARP1 would enhance ROS formation due to continuous NQO1 futile redox cycling of β-lap and generate greater DNA damage that, in turn, would not be repaired due to concomitant PARP inhibition. A549 NSCLC cells were pre-treated with nonlethal doses of various PARP inhibitors, including Rucaparib (Figure 3A), Olaparib (Figure 3B), and Veliparib (Figure 3C), each at 15 μM, or 1.25 μM Talazoparib (Figure 3D) (nontoxic inhibitor doses were tested, Figure S3A–S3D) for 2 hr, followed by co-treatment with relatively nontoxic β-lap doses (1–4 μM) + PARP inhibitors for an additional 2 hr. Drugs were removed and cells assessed for survival. Rucaparib, Olaparib and Talazoparib (at $<LD_{10}$ doses, Figure S3A–S3D) dramatically increased the sensitivities of A549 cells to otherwise nonlethal β-lap doses (Figures 3A–3D), resulting in dose enhancement ratios (DERs) that were proportional to PARP inhibition in cells (Figures 3E–3J) or using purified PARP1 in vitro (Figure S3E–S3G). Dose-response studies for each PARP inhibitor confirmed that optimal synergistic lethality with β-lap was noted at 15 μM for Rucaparib

and Olaparib, while Talazoparib was potent at 1.25 μM. Veliparib was the least potent and effective PARP inhibitor for synergy with β-lap (Figure S3H–S3K). Synergy (Chou and Talalay, 1984) was found for β-lap + Rucaparib, Olaparib, or Talazoparib at eta (η) values of 0.452, 0.494, and 0.584, respectively. Dicoumarol (DIC, 50 μM, 2 hr) prevented all synergy responses (Figure S3H–S3K). We chose Rucaparib for further studies since clinical grade formulation was available.

To delineate the relationship between NQO1 and *CAT* in β-lap lethality, clones varying in NQO1 expression showed that ~100 units of NQO1 enzyme activity were needed (Figure S3L). In contrast, LD_{50} values dramatically increased in cells with <100 units of NQO1.

We examined NSCLC, PDA, and breast cancer cells that were reconstituted or knocked down for NQO1 expression, ± dicoumarol (Figures 4A–4H). H596 NSCLC cells that lack NQO1 expression due to a *2 *NQO1* polymorphism, were reconstituted for NQO1 (Bey et al., 2007) and sensitized to Rucaparib + β-lap. Dicoumarol suppressed lethality after β-lap alone, or in synergy with Rucaparib (Figures 4A, 4B). MiaPaCa2 PDA cancer cells express significant KRAS-driven NQO1 levels and were hypersensitive to Rucaparib + β-lap (Figure 4C), with dicoumarol suppression. Stable MiaPaCa2 NQO1 knockdown clones, 17-7 (Figure 4D) or 17-3 (Figure S4A, S4B), were significantly resistant to the drug combination vs MiaPaCa2 shRNA vector only clones that were as hypersensitive as parental MiaPaCa2 cells to Rucaparib + β-lap; MiaPaCa2 knockdown clones were described (Li et al., 2011). Similarly, β-lap-, chemo-, and radio- resistant Suit-2 (S2-013) PDA cancer cells that lack NQO1 expression due to a *2 polymorphism, were rendered hypersensitive to β-lap + Rucaparib treatments with re-expression of wild-type NQO1. Dicoumarol suppressed synergy (Figure 4E). NQO1 expression in S2-013 cells was confirmed by Western blotting (inset, Figure 4E). NQO1-deficient S2-013 cells were resistant to Rucaparib + β-lap or β-lap alone (Figure 4F). Finally, β-lap-resistant *2 *NQO1* polymorphic MDA-MB-231 TNBC cells were rendered hypersensitive to Rucaparib + β-lap after NQO1 expression was restored, but blocked by dicoumarol (Figure 4G). *NQO1*$^{-}$ MDA-MB-231 cells were inherently resistant to β-lap, with or without Rucaparib (Figure 4H). All Rucaparib doses were nontoxic (Figure S4C), and NQO1 levels in genetically matched NQO1-expressing or -deficient H596, MiaPaCa2, or MDA-MB-231 cells were described (Bey et al., 2007; Huang et al., 2012; Li et al., 2011). Synergy between PARP inhibitors and β-lap was noted across cell lines and independent of oncogenic driver mutations (Figure 2 and Figure S4D).

Inhibition of PARP1 hyperactivation is required to mediate synergistic apoptosis with β-lapachone

MCF-7 cells were hypersensitive to Rucaparib (15 μM) + β-lap (2 μM) treatments for 2 hr, in an NQO1-dependent manner (Figure 5A). Note a synergistic (η=0.452) log-increase in lethality from 25% survival with β-lap (2 μM, 2 hr) alone to <2% survival with the drug combination, where Rucaparib alone was nonlethal. A rapid increase and continuous level of high molecular weight PARylated PARP1 protein (PAR-PARP1), along with lowered but sustained NAD^+/ATP levels were noted after a sublethal 2 μM β-lap dose alone (Bey et al., 2013). A lethal dose of β-lap (5 μM) hyperactivated PARP1, with a rapid rise of PAR formation that dissipated by ~15 min due to dramatic NAD^+ loss and simultaneous PAR

glycohydrolase (PARG) activity (Bey et al., 2007). Co-addition of Rucaparib dramatically suppressed PAR formation (Figure 5B). PARP1 inhibition by Rucaparib was accompanied by earlier and significantly greater DSBs (γH2AX foci/nucleus, Figure 5C), suggesting that initial β-lap-induced DNA base damage and SSBs detected and normally repaired by PARP1 were converted to lethal DSBs. Hyperactivation of PARP1 by lethal β-lap doses (5 μM, <2% survival) was accompanied by a dramatic NAD^+ loss reversed by Rucaparib (Figure 5D). Addition of Rucaparib to a sublethal β-lap dose (~25% survival) mitigated NAD^+ losses and dicoumarol reversed all effects (Figure 5D).

We stably depleted PARP1 levels in MCF-7 cells using lentiviral shRNA knockdown and noted significant suppression of β-lap-induced PAR formation (Figure 5E). Dramatic loss of ATP nucleotides occurred during β-lap-induced PARP1 hyperactivation (Figure 5F). Loss was blocked by dicoumarol, and ATP levels remained fairly stable during drug treatment (Figure 5F), showing that ATP loss caused by β-lap was largely a result of PARP1 hyperactivation. PARP1 knockdown caused a dramatic increase in lethality in β-lap-treated stable shPARP1 knockdown MCF-7 cells (Figure S4E), with resistance to ATP losses (Figure S4F). The lethal effects of β-lap, with or without PARP1 inhibition or knockdown, were NQO1-dependent and blocked by dicoumarol (Figure S4E). Near identical synergistic results were noted in β-lap-exposed stable shPARP1 vs shSCR MDA-MB-231 TNBC cells (Figure S4G–S4J).

Synergy results from β-lapachone-induced, NQO1-mediated, tumor-selective DNA damage and PARP inhibition

Exposure of A549 cells to 3 μM β-lap alone for 2 hr represents a sublethal dose (>70% survival), whereas >5 μM β-lap treatments were lethal (Bey et al., 2007) (Figure S5A–S5D. Dicoumarol blocked all β-lap-induced responses (Figure S5A). A nonlethal Rucaparib dose (15 μM, 4 hr) resulted in synergistic lethality with 3 μM β-lap (<1% survival) (Figure S5A). NQO1-mediated H_2O_2 levels produced in the first 2 hr exposure of A549 cells to Rucaparib (15 μM) + β-lap (3 μM) were similar to those produced cells exposed to a sublethal dose of β-lap (3 μM) (Figure 6A). A sublethal dose of β-lap alone (3 μM) or in combination with synergistic doses of Rucaparib (15 μM), resulted in equivalent oxygen consumption rates (OCRs) (Figure 6B), suggesting that these doses of β-lap caused significant cell stress, but cells were able to keep up with the demand for $NAD(P)H/NAD(P)^+$, without PARP1 hyperactivation. At a higher β-lap dose (8 μM), NQO1 futile redox becomes exhausted with dramatic decay in OCRs (Figure 6B) as NAD^+ levels dramatically dropped due to extensive PARP1 hyperactivity (Figures 6C, S5B). When Rucaparib was added with 8 μM β-lap, NQO1 futile redox cycling was refueled and sustained OCRs resulted (Figure 6B). Total NAD^+ and NADH levels decreased after exposure to β-lap (8 μM) alone as a direct result of PARP1 hyperactivation. β-Lap-induced NAD^+ and NADH losses were rescued by Rucaparib (Figure 6C), consistent with suppression of PARP1 activity/hyperactivation monitored by PAR formation ± Rucaparib (Figure S5B). Similarly, ATP depletion mirrored changes in total NAD^+ and NADH after β-lap alone and with Rucaparib (Figure 6D). Controls for Rucaparib included inhibition of PAR formation (Figure S5B), synergistic killing of β-lap-treated A549 cells in an NQO1-dependent manner (Figure S5A) and selective killing of BRCA2-deficient CAPAN-1 PDA cells (Figure S5C). Rucaparib did not alter NQO1

activities (Figure S5D). Overall, at sublethal β-lap doses (~3 μM) where synergy was noted with Rucaparib (Figure S5A), moderate OCRs were maintained (Figure 6B) for the entire 2 hr treatment time due to sustained NAD^+/ATP and NADH pools that continuously supply H_2O_2 stress and DNA damage that were not repaired due to PARP inhibition (Figures 6B, 6C). This mechanism was most visible after a lethal dose of β-lap (8 μM) ± Rucaparib (15 μM, 4 hr) treatment (open circle vs closed diamond, Figure 6B).

PARP inhibition amplifies NQO1-dependent DNA damage induced by β-lapachone

Alkaline comet assays were used to detect β-lap-induced total DNA damage (e.g., abasic sites, SSBs, DSBs), which were significantly higher in A549 cells after exposure to β-lap (3 μM) + Rucaparib (15 μM) vs β-lap or Rucaparib alone (Figure 7A). Combined exposure of these two agents was not statistically different from exposure to a supralethal dose of β-lap (8 μM) (Figure 7A, 7B). Since similar ROS levels were noted with the combination therapy vs individual exposures of A549 cells to low doses of β-lap alone (Figure 6A), our data strongly suggest that inhibiting PARP activity by Rucaparib significantly impeded the repair of initial β-lap-induced DNA lesions (DNA base, SSBs (Dong et al., 2010; Li et al., 2011)), culminating in conversion of initial lesions to more lethal non-repairable DSBs noted 24 hr later (Figure 7B).

PARP1 inhibition provides a molecular switch, converting programmed necrosis to apoptosis

Treatment of MCF-7 cells with a lethal dose of β-lap alone (5 μM) caused atypical PARP1 and p53 proteolytic cleavage, diagnostic of programmed necrosis (lane 6, Figure 7C). Caspase activation was not observed and addition of the pan-caspase inhibitor, zVAD-fmk, had no influence on proteolysis or cell death (lane 7, Figure 7C). In contrast, under the synergistic conditions of Rucaparib (15 μM, 2 hr) + Rucaparib (15 μM) + β-lap (2 μM) for 2 hr, MCF-7 cells (Figure 5A), showed typical caspase-mediated cleavage of PARP1 and caspase 7 proteolysis that were efficiently blocked by zVAD-fmk (lanes 4 vs 5, Figure 7C). Cell death in MCF-7 cells after Rucaparib + β-lap was similar to responses of these cells to Staurosporine (STS, lanes 8–9, Figure 7C). Similarly, A549 NSCLC and MiaPaCa2 PDA cells exposed to Rucaparib + β-lap for 2 hr resulted in caspase 3/7-mediated proteolysis that was blocked by zVAD-fmk (Figure 7D). Cleavage of caspase 3 to an active form was confirmed in A549 cells exposed to Rucaparib + β-lap, indicating apoptosis as found with STS exposure (Figure S5E). Exposure of cells to low doses of Rucaparib or β-lap alone did not elicit cell death or proteolysis. Treatment of these cells with a high dose of β-lap (8 μM, 2 hr) did not stimulate caspase activation (Figure 7D).

Analyses of biomarkers confirm synergistic responses in mouse tumor models after Rucaparib + β-lapachone

MiaPaCa2 orthotopic xenografts (1×10^6 cells injected into pancreas), using 4 X more cancer cell burden than previously performed (Li et al., 2011), were formed in NOD/SCID female mice (20–22 g) to examine synergy. Mice were treated with: vehicle (HPβCD, iv, tail vein); HPβCD-β-lap (hereafter referred to as β-lap, at 10, 15 or 22 mg/kg, iv) alone; Rucaparib (15 mg/kg, ip) alone; or Rucaparib (15 mg/kg, ip) 2 hr prior to β-lap (10, 15, 22 mg/kg, iv). Treatments were given every day for five days, with seven days rest, and

repeated for another five days (i.e., M-F for two weeks, 10 injections total). Mice were then monitored for changes in tumor volumes (Figure 8A), weight loss (Figure S6A), overall survival (Figures 8B, S6B and S6C), metastases to liver (Figure 8C), and alterations in PAR and γH2AX formation (Figure 8D) and NAD^+/ATP losses (Figure 8E). Treatment with HPβCD-β-lap alone caused dramatic increases in PAR formation in MiaPaCa2 tumor tissue, that were abolished by Rucaparib co-addition, and delayed γH2AX-indicated DSBs were noted (Figures 8D, S6D). Elevated and early formation of γH2AX-indicated DSBs in MiaPaCa2 tumor tissue were noted in mice treated with Rucaparib + β-lap (Figure 8D), with spared losses in NAD^+/ATP pools (Figure 8E). In contrast, normal tissue remained nonresponsive to any β-lap exposure, ± Rucaparib (Figure 8D). Pharmacokinetic (PK) analyses revealed no alterations in β-lap or Rucaparib drug levels in blood or tumor tissue of mice treated with combination vs single agent therapy, but Rucaparib levels in both groups were significantly elevated (nearly 10-fold) in tumor vs plasma tissue over time (Figure S6E–S6H), as reported (Murray et al., 2014). A significant and synergistic antitumor dose-response was noted with Rucaparib + β-lap from 15–22 mg/kg (Figure 8A), with accompanied reduction in the number of metastatic nodules to livers (Figure 8C).

Alterations in antitumor activities and metastasis prevention correlated well with synergistic survival in MiaPaCa2 xenograft-containing mice with Rucaparib + β-lap (Figures 8B,C, S6B and S6C). Note that doses of Rucaparib alone were not effective, as MiaPaCa2 is not a BRCA1/2 mutant tumor. While β-lap caused efficacious antitumor activities at 15 and 22 mg/kg, significantly improved and synergistic antitumor responses were noted when Rucaparib was added (Figures 8B, S6B and S6C).

Similar improved antitumor responses were noted in Rucaparib + β-lap-treated A549 orthotopic xenografts (~1×10^6 cells, tail vein) in NOD/SCID female mice (Figure S7A–S7F). Treatments were given every other day for 5 injections over 10 days. Bioluminescence imaging (BLI) and survival were used to monitor tumor growth and responses (Figure S7A–S7F). Individual tumor volume waterfall plots were graphed (Figure S7G). Exposure to Rucaparib or β-lap alone resulted in decreased growth, and enhanced the survival of A549-bearing mice, although all mice succumbed to tumor burden by day 155 (Figure S7C). Individual tumor volumes showed signs of cytostatic tumor growth suppression rather than significant regression (Figure S7G). In contrast, mice treated with Rucaparib + β-lap showed synergistic antitumor activity and a significant survival over single agents alone, with one mouse apparently cured (Figure S7A–S7F). The MiaPaCa2 and A549 data showed significant synergy at three doses of each agent (η=0.86; SEM=0.33) (Chou and Talalay, 1984; Lee et al., 2007). Rucaparib + β-lap showed no signs of methemoglobinemia (i.e., labored breathing, lethargy in 45 min), noted with higher doses of β-lap (~30 mg/kg, iv) alone (Blanco et al., 2010; Huang et al., 2012). No significant weight loss or long-term normal tissue toxicities (liver, lung, pancreas, kidney, spleen, colon, etc.) by histopathology at 45 days post-treatment were noted; the livers of treated mice are shown as NQO1 levels are highest in livers of normal mice (Figure S7H). Synergistic antitumor activity was noted at lower doses of Rucaparib (2.5 mg/kg) with β-lap (22 mg/kg) (Figure S7I). The meager efficacy of Rucaparib alone at 10 mg/kg was variable against A549 xenografts, as in Figure S7I. Elevated PARP hyperactivation (PAR) and delayed DSB formation were noted after β-lap alone, while suppressed PAR formation (PARP1 inhibition) and earlier and greater DSB

formation (elevated γH2AX) were noted after Rucaparib + β-lap (Figure S7D, S7J). Consistent with a switch from β-lap-induced programmed necrosis in *NQO1*$^+$ A549 NSCLC tumors, dramatic NAD^+ and ATP losses were noted after β-lap (22 mg/kg) alone (Figure S7E, S7F), but were blocked (NAD^+/ATP levels maintained) by Rucaparib. *NQO1*$^+$ A549 tumors were killed by DSB-induced apoptosis, as per elevated γH2AX levels in tumor (Figure S7D, S7J). Responses in associated normal tissue to β-lap alone (small but significant PAR formation increase at 90 min) were significantly suppressed by Rucaparib, but without a major increase in γH2AX (Figure S7D, S7J). Pharmacokinetics showed that co-addition of Rucaparib + β-lap did not alter β-lap blood or tumor pools (Figure S7K, S7L). Rucaparib blood and tumor pharmacokinetics were not altered by β-lap (Figure S7K, S7M) and a significant accumulation (>10-fold) of Rucaparib in tumor tissue (Figure S7M), as noted in MiaPaCa2 xenografts (Figure S6G, S6H), using 15 mg/kg ip bolus injections was noted (Murray et al., 2014).

Discussion

Here, we show that combining PARP inhibitors with the highly tumor-specific DNA damaging agent, β-lap, results in synergy at nontoxic doses of both drugs in *NQO1*$^+$ over-expressing non-small cell lung (NSCLC), pancreatic ductal adenocarcinoma (PDA) and breast cancers, including TNBC. The combination exploits a unique therapeutic window driven by elevated *NQO1:CAT* ratios in solid cancers. Combining a PARP inhibitor with β-lap results in robust, NQO1-dependent, tumor-selective SSBs, DSBs and apoptosis in vitro and in vivo, with synergistic antitumor efficacy in mice bearing *NQO1*$^+$ pancreatic or NSCLC orthotopic xenografts. Mechanistically, β-lap-induced DNA lesion formation was significantly enhanced by: (**i**) maintained levels of NAD(P)H pools that constantly refueled NQO1 redox cycling of the drug; and (**ii**) blocked DNA repair due to PARP inhibition. While β-lap addition afforded NQO1-selectivity to PARP inhibitors, the combination significantly lowered the efficacious dose of β-lap, wherein dose-limiting methemoglobinemia was avoided. Normal tissues were spared due to their extremely low *NQO1:CAT* ratios.

The mechanism of action of β-lap (ARQ761) offers unique features that can be exploited for synergy with DNA repair inhibitors or specific damaging agents. NQO1 bioactivatable drugs are ideally suited to exploit elevated *NQO1:CAT* ratios in tumors via generation of supralethal H_2O_2 levels. Low *NQO1:CAT* ratios in normal tissue offer protection, even from the drug's robust H_2O_2-mediated bystander effects (Cao et al., 2014). β-Lap should avert drug resistance in NQO1 over-expressing cancers, while allowing tumor-selective therapies of recalcitrant PDA and NSCLC cancers. Analyses of NSCLCs growing >140 days post-Rucaparib + β-lap revealed *NQO1*$^+$ and no *NQO1*$^-$ cancers, suggesting an effect of insufficient drug levels rather than resistance. These drugs will be particularly effective against early neoplasms that over-express NQO1, as in pancreatic intraepithelial neoplasia (PanINs). Unlike other anticancer agents, cells exposed to β-lap exhibit lethal responses independent of cell cycle, p53 status (Bey et al., 2007; Bey et al., 2013; Moore et al., 2015; Planchon et al., 2001) and/or oncogenic driver or passenger mutations. All responses derive from NQO1-dependent futile redox cycling of the drug, where NQO1 expression/activity loss (by *2 or *3 alterations) results in considerable inherent resistance, but re-introduction

of *NQO1* restores hypersensitivity. Of note are the fairly uniform LD_{50} values (1–5 μM) for β-lap across individual cancer subtypes, even between cancers of different origins (e.g., NSCLC, PDA and breast.

PARP inhibitors offered synergistic killing of $NQO1^+$ cancers, including lung, pancreas and breast. Selective suppression of PARP1 expression, without affecting PARP2 levels (Dong et al., 2010), using shRNA-specific knockdown in MCF-7 and MDA-MB-231 cells, strongly suggests that PARP1 is the most critical target, consistent with inhibitory effects on PAR-PARP1 formation and NAD^+/ATP losses. PARP inhibitors prevented NAD^+ loss, sustained NQO1 futile cycling of β-lap, caused elevated ROS/H_2O_2 levels with enhanced DNA damage (e.g., DSBs), whose repair was suppressed by PARP inhibition. Cell death switched from caspase-independent programmed necrosis by β-lap alone to NQO1-selective caspase-mediated apoptosis after PARP inhibitors + β-lap. The switch in mechanism from PAR formation and programmed necrosis to DSB-induced apoptosis was noted in vitro and in vivo. Importantly, combination therapy permitted use of lowered efficacious doses of β-lap, avoiding clinically significant dose-limiting methemoglobinemia.

β-Lap afforded tumor-selective use of PARP inhibitors, selectively killing $NQO1^+$, while sparing $NQO1^-$ cells/tissues. Synergy between PARP inhibitors and β-lap increased efficacy to kill cells independent of p53 status, or overall oncogenic driver mutations. MCF-7 and MDA-MB-231 cells were equally sensitized by Rucaparib + β-lap, yet these cells have wild-type vs mutant p53 and estrogen receptor+ vs triple-negative (estrogen receptor-, Heregulin receptor 2- and progesterone receptor-) growth statuses, respectively. The drug combination retains NQO1-dependency, where synergy was noted in >90% mutant KRAS PDAs, but also equally effective against >80% NSCLC, >60% breast, >60% prostate, >45% head and neck and >60% colon cancers, where NQO1 is elevated. In contrast, normal tissue that typically express little or no NQO1 were resistant to NQO1 bioactivatable drugs.

Thus, this drug combination will greatly expand the efficacious use of PARP inhibitors to additional $NQO1^+$ cancers (Siegel and Ross, 2000). Anti-apoptotic mechanisms might arise in tumors in response to PARP inhibitor + β-lap therapy. However, overall cell death is still triggered by PARP inhibitors + β-lap by excessive levels of H_2O_2, at doses not likely to elicit resistance. We have not observed resistance to β-lap or other NQO1 bioactivatable drugs in $NQO1^+$ cancer cells, even when 75% $NQO1^-$ cells were co-cultured with 25% $NQO1^+$ cells (Cao et al., 2014).

Our results have immediate translational applicability. β-Lap is relatively new in clinical trials (ARQ761), but has shown promising tolerability, pharmacokinetics and responses (Gerber et al., 2014). Prior and ongoing clinical trials showed PARP inhibitors were well-tolerated in clinical use, and one (Olaparib) recently FDA approved for treatment of advanced ovarian cancer (Lee et al., 2014). Based on our preclinical studies in vivo, concomitant synergy in toxicity was not noted vs individual agents (β-lap or Rucaparib) alone, so that β-lap and Rucaparib markedly enhanced antitumor activity, improved survival vs either agent alone, but ultimately resulted in no increase in toxicity to normal tissue or showed increased toxic side-effects. Rucaparib shows tumor-selective accumulation, ± β-lap, and does not affect β-lap pharmacokinetics. Leveraging NQO1 bioactivatable drugs to

afford a significantly broader, tumor-selective use of PARP inhibitors in clinical trials is warranted.

Methods

Cell Culture

Breast and PDA cancer cells were obtained from the American Tissue Culture Collection (ATCC, Manasas, VA) and lung cancer cells were generated by the UTSW-MD Anderson SPORE in lung cancer (Skoulidis et al., 2015) or were from the ATCC. Cells were grown as in Supplemental Materials and Methods.

NQO1 Enzyme Activity Assays

NQO1 enzyme activities from cancer cells or tumor or normal tissues were measured as dicoumarol-inhibited units (Li et al., 2011; Pink et al., 2000).

Cell-based PARP Enzymatic Activity Inhibition Assays

Briefly, A549 cells were pre-treated with varying concentrations (0, 1.0, 2.5, 5.0, 10, and 15 μM) of PARP inhibitors (Rucaparib or Olaparib) for 2 hr followed by co-treatment with vehicle (DMSO) or β-Lap (3 μM) for 2 hr. Cells were washed with ice-cold PBS twice and lysed with ice-cold RIPA buffer containing protease inhibitor cocktails. Total lysate protein concentrations were determined by BCA assays for equal loading onto 4–20% gradient gels and Western blotting to probe for PARP inhibition via PAR formation. α-Tubulin was used as loading control. PAR formation densitometry was measured via NIH ImageJ, and PARP1 activity was measured for each PARP inhibitor concentration relative to control with β-lap (3 μM). Linear regression/correlation was calculated via Prism 7.

Dose Enhancement Ratio (DER) Calculations

DER calculations were obtained using the equation below:

$$\mathbf{DER} = \frac{[\beta\text{-Lap}]_{3\mu M,\ \%\text{Cell Survival}}}{([\beta\text{-Lap}]_{3\mu M} + [\underline{\text{PARPi}}])_{\%\text{Cell Survival}}}$$

$$[\text{PARPi}] = 0, 1, 2.5, 5.0, 10, 15\ \mu M$$

Relative Cell Survival (%) of β-lap (3 μM) alone or combinations [β-lap (3 μM) + PARP inhibitor concentrations (0, 1.0, 2.5, 5.0, 10, 15 μM) of Rucaparib and Olaparib] were obtained via DNA assays. Mean values were used in the equation above to calculate DERs. Linear regression/correlation was calculated via Prism 7 software.

Survival Assays

Relative survival assays based on 7-day DNA content assessments were described (Huang et al., 2012; Pink et al., 2000). Colony forming ability assays were performed using 500–1000 cells per 60 mm plates. Colonies of >50 healthy appearing cells were counted and normalized to vehicle-treated cells.

ATP, NAD/NADH and H_2O_2 Quantification

ATP (CellTiter-Glo), hydrogen peroxide (H_2O_2) (ROS-Glo), and NAD/NADH (NAD/NADH-Glo) were assayed at indicated time-points during or after treatments using specific assays (Promega, Madison, WI).

Antibodies

Antibodies used for immunofluorescence and Western blotting, included: NQO1 (A180), PARP1 (SC-8007, Santa Cruz, La Jolla, CA), Actin (C4, Santa Cruz), PAR (Trevigen, Gaithersburg, MD), Cleaved caspase 7 (D6H1, Cell Signaling, Danvers, MA), cleaved caspase 3 (5A1E, Cell Signaling), p53 (DO-1, Santa Cruz), catalase (D4P7B, Cell Signaling), γH2AX (JBW301, Millipore, Temecula, CA), and α-tubulin (Santa Cruz).

Western Blotting

Westerns were performed using ECL chemiluminescent detection and density analyses using NIH ImageJ with intensity normalization (Bey et al., 2007; Huang et al., 2012; Li et al., 2011).

Comet and Immunofluorescence Assays

Alkaline comet assays (Trevigen) to measure total DNA damage, including DNA base, SSBs and DSBs were assessed (Bey et al., 2007). Slides were stained with SYBR green and images captured using a Leica DM5500 microscope. Comet tail lengths were quantified by NIH Image J. Cells were imaged by immunofluorescence for γH2AX foci on a Leica DM5500 fluorescent microscope and quantified for foci/nucleus (Bey et al., 2007; Huang et al., 2012; Li et al., 2011).

Oxygen Consumption Rate (OCR) Assessments

Real-time OCRs measurements were monitored using the Seahorse XF bioanalyzer (Seahorse Bioscience, Billerica, MA) in Seahorse media containing glucose and glutamine.

Antitumor, Survival, Pharmacokinetic and Pharmacodynamic Studies

Antitumor, survival, pharmacodynamics and pharmacokinetic studies using pancreatic-specific orthotopic MiaPaCa2 xenograft-bearing NOD/SCID mice were performed. All animal procedures were approved by the UT Southwestern IACUC committee. Rucaparib for in vivo use was obtained from Clovis Oncology. Bioluminescence (BLI)-based tumor volumes, long-term survival and target validation assays were performed with log-rank tests for survival (Blanco et al., 2010; Ma et al., 2015). Pharmacokinetics (PK) of Rucaparib or β-lap levels in blood and tumor were assessed by LC-MS/MS analyses following extraction of plasma or tumor homogenates with acetonitrile (Blanco et al., 2010; Ma et al., 2015). An unpaired t-test (GraphPad QuickCalcs, San Diego, CA) was used significant differences in β-lap concentrations after different treatments. Pharmacodynamic (PD) parameters of PAR formation, γH2AX, and NAD^+/ATP levels in tumors were performed (Ma et al., 2015).

Microarray Expression Data, Processing and Analyses

Gene expression data series were retrieved from Gene Expression Omnibus (GEO) database using criteria described in Supplemental Methods. The assembled cohort included 327 NSCLC tumor, 105 normal lungs and 128 NSCLC cell line specimens, for a total of 560 specimens. Matched-pair specimens (n=105) from two independent studies were analyzed. The 560 specimen data files were downloaded as raw CEL files (Irizarry et al., 2003). R package aroma.affymetrix was used and data processed using the linear model from RMA, then fit robustly using probe level models (Robinson and Speed, 2007). Probe level models were fit to RMA-background corrected and quantile normalized data to obtain gene-level summaries. Gene-level summarization used standard CDF provided by Affymetrix. The Welch's t-test for unequal variance was used to compute p value for the difference in means. All analyses were performed in R. Statistical tests were performed using base R statistical functions, graphics were generated using the ggplot2 graphics package (Wickham, 2009).

Statistics

Data (means, ± standard deviations) were graphed and ANOVA used to compare groups. Two-tailed Student's t-tests for independent measures with Holm-Sidak correction for multiple comparisons, if >1 comparisons, were performed. Minimum replicate size for any experiment was n=3. Alpha was set to 0.05. Statistical analyses were performed in GraphPad Prism 6. Images were representative of results of experiments or stainings repeated 3X. *p<0.05; **p<0.01 and ***p<0.001.

Synergy Calculations

Synergy interactions between two drugs were evaluated using two methods: 1) Direct comparisons made between the effect of combined treatments and the effect of individual drugs in each experiment (Figures 3A, 3B and 3D; Figures 4A, 4C, 4E and 4G; Figure 5A; Figures S3H, S3I and S3K); and 2) Formal synergy effects evaluations used a strict method proposed by Chou and Talalay and Lee et al. (Chou and Talalay, 1984; Lee et al., 2007), where pooled, multiple dose-responses for each treatments were required. Values (eta, η) were reported based on multiple dose-responses data from studies in Figures 3A, 3B and 3D; Figures 4A, 4C, 4E and 4G; Figures 5A; and S3H, S3I and S3K. We formally tested drug-drug interactions for three pairs: a) β-Lap + Rucaparib showed a highly significant effect of (η=0.452, p value=0.0003); b) β-Lap + Olaparib showed a highly significant effect of synergy (η=0.494, p value=0.0013); and c) β-Lap + Talazoparib showed a significant synergy (η=0.584, p value=0.036). For in vivo Rucaparib + β-lapachone synergy showed an η value of 0.86, with p values indicated on graphs.

Supplementary Material

Refer to Web version on PubMed Central for supplementary material.

Acknowledgments

Special thanks to Dr. Julia Meade for her review. We are grateful to UTSW SCCC (5P30CA142543) for support of cores (Bioinformatics, Biomarker Research, and Preclinical Pharmacology (PK)). Preclinical Pharmacology Core was supported by institutional funds from the Institute for Innovations in Medical Technology (IIMT) and CPRIT

(RP110708-C3) to NSW. Work in NSCLC and breast cancers were supported by NCI (CA102792) to DAB and UTSW-MD Anderson SPORE in lung cancer to JDM. Work in PDA was supported by AACR/PanCan Grants 12-60-25-BOOT and 15-65-25-BOOT to DAB. DAB, YD and EAB declare US patent application, 'Methods of treating cancer comprising targeting *NQO1*' (13/820,127). DAB, XH and ZRM declare US patent applications, 'Compounds and anti-tumor NQO1 substrates (14/351, 8961) and 'Tumor-selective combination therapy' (TF13048; international PCT/US2014/033400). DEG receives funding for clinical trials from ArQule, Inc., grants SCCC-10Y11 ARQ-761 and SCCC-15Y11.

References

Albert JM, Cao C, Kim KW, Willey CD, Geng L, Xiao D, Wang H, Sandler A, Johnson DH, Colevas AD, et al. Inhibition of poly(ADP-ribose) polymerase enhances cell death and improves tumor growth delay in irradiated lung cancer models. Clinical Cancer Research. 2007; 13:3033–3042. [PubMed: 17505006]

Bey EA, Bentle MS, Reinicke KE, Dong Y, Yang CR, Girard L, Minna JD, Bornmann WG, Gao J, Boothman DA. An NQO1- and PARP-1-mediated cell death pathway induced in non-small-cell lung cancer cells by beta-lapachone. Proc Natl Acad Sci USA. 2007; 104:11832–11837. [PubMed: 17609380]

Bey EA, Reinicke KE, Srougi MC, Varnes M, Anderson VE, Pink JJ, Li LS, Patel M, Cao L, Moore Z, et al. Catalase abrogates beta-lapachone-induced PARP1 hyperactivation-directed programmed necrosis in NQO1-positive breast cancers. Molecular Cancer Therapeutics. 2013; 12:2110–2120. [PubMed: 23883585]

Blanco E, Bey EA, Khemtong C, Yang SG, Setti-Guthi J, Chen H, Kessinger CW, Carnevale KA, Bornmann WG, Boothman DA, Gao J. Beta-lapachone micellar nanotherapeutics for non-small cell lung cancer therapy. Cancer Research. 2010; 70:3896–3904. [PubMed: 20460521]

Cao L, Li LS, Spruell C, Xiao L, Chakrabarti G, Bey EA, Reinicke KE, Srougi MC, Moore Z, Dong Y, et al. Tumor-Selective, Futile Redox Cycle-Induced Bystander Effects Elicited by NQO1 Bioactivatable Radiosensitizing Drugs in Triple-Negative Breast Cancers. Antioxidants & Redox Signaling. 2014; 21:237–250. [PubMed: 24512128]

Chou TC, Talalay P. Quantitative analysis of dose-effect relationships: the combined effects of multiple drugs or enzyme inhibitors. Adv Enzyme Regul. 1984; 22:27–55. [PubMed: 6382953]

Dantzer F, de La Rubia G, Menissier-De Murcia J, Hostomsky Z, de Murcia G, Schreiber V. Base excision repair is impaired in mammalian cells lacking Poly(ADP-ribose) polymerase-1. Biochemistry. 2000; 39:7559–7569. [PubMed: 10858306]

Dong Y, Bey EA, Li LS, Kabbani W, Yan J, Xie XJ, Hsieh JT, Gao J, Boothman DA. Prostate cancer radiosensitization through poly(ADP-Ribose) polymerase-1 hyperactivation. Cancer Research. 2010; 70:8088–8096. [PubMed: 20940411]

Farmer H, McCabe N, Lord CJ, Tutt AN, Johnson DA, Richardson TB, Santarosa M, Dillon KJ, Hickson I, Knights C, et al. Targeting the DNA repair defect in BRCA mutant cells as a therapeutic strategy. Nature. 2005; 434:917–921. [PubMed: 15829967]

Helleday T, Petermann E, Lundin C, Hodgson B, Sharma RA. DNA repair pathways as targets for cancer therapy. Nature Reviews Cancer. 2008; 8:193–204. [PubMed: 18256616]

Huang X, Dong Y, Bey EA, Kilgore JA, Bair JS, Li LS, Patel M, Parkinson EI, Wang Y, Williams NS, et al. An NQO1 substrate with potent antitumor activity that selectively kills by PARP1-induced programmed necrosis. Cancer Research. 2012; 72:3038–3047. [PubMed: 22532167]

Irizarry RA, Hobbs B, Collin F, Beazer-Barclay YD, Antonellis KJ, Scherf U, Speed TP. Exploration, normalization, and summaries of high density oligonucleotide array probe level data. Biostatistics. 2003; 4:249–264. [PubMed: 12925520]

Jacob DA, Bahra M, Langrehr JM, Boas-Knoop S, Stefaniak R, Davis J, Schumacher G, Lippert S, Neumann UP. Combination therapy of poly (ADP-ribose) polymerase inhibitor 3-aminobenzamide and gemcitabine shows strong antitumor activity in pancreatic cancer cells. J Gastroenterology and Hepatology. 2007; 22:738–748.

Kolesar JM, Kuhn JG, Burris HA3rd. Detection of a point mutation in NQO1 (DT-diaphorase) in a patient with colon cancer. J National Cancer Institute. 1995; 87:1022–1024.

Lee JJ, Kong M, Ayers GD, Lotan R. Interaction index and different methods for determining drug interaction in combination therapy. J Biopharm Stat. 2007; 17:461–480. [PubMed: 17479394]

Lee JM, Ledermann JA, Kohn EC. PARP Inhibitors for BRCA1/2 mutation-associated and BRCA-like malignancies. Annals of Oncology. 2014; 25:32–40. [PubMed: 24225019]

Li LS, Bey EA, Dong Y, Meng J, Patra B, Yan J, Xie XJ, Brekken RA, Barnett CC, Bornmann WG, et al. Modulating endogenous NQO1 levels identifies key regulatory mechanisms of action of beta-lapachone for pancreatic cancer therapy. Clinical Cancer Research. 2011; 17:275–285. [PubMed: 21224367]

Ma X, Huang X, Moore Z, Huang G, Kilgore JA, Wang Y, Hammer S, Williams NS, Boothman DA, Gao J. Esterase-activatable beta-lapachone prodrug micelles for NQO1-targeted lung cancer therapy. J Controlled Release. 2015; 200:201–211.

Moore Z, Chakrabarti G, Luo X, Ali A, Hu Z, Fattah FJ, Vemireddy R, DeBerardinis RJ, Brekken RA, Boothman DA. NAMPT inhibition sensitizes pancreatic adenocarcinoma cells to tumor-selective, PAR-independent metabolic catastrophe and cell death induced by beta-lapachone. Cell Death & Disease. 2015; 6:e1599. [PubMed: 25590809]

Murray J, Thomas H, Berry P, Kyle S, Patterson M, Jones C, Los G, Hostomsky Z, Plummer ER, Boddy AV, Curtin NJ. Tumour cell retention of rucaparib, sustained PARP inhibition and efficacy of weekly as well as daily schedules. British J Cancer. 2014; 110:1977–1984.

Pink JJ, Planchon SM, Tagliarino C, Varnes ME, Siegel D, Boothman DA. NAD(P)H:Quinone oxidoreductase activity is the principal determinant of beta-lapachone cytotoxicity. J Biological Chemistry. 2000; 275:5416–5424.

Planchon SM, Pink JJ, Tagliarino C, Bornmann WG, Varnes ME, Boothman DA. beta-Lapachone-induced apoptosis in human prostate cancer cells: involvement of NQO1/xip3. Exp Cell Research. 2001; 267:95–106.

Rajan A, Carter CA, Kelly RJ, Gutierrez M, Kummar S, Szabo E, Yancey MA, Ji J, Mannargudi B, Woo S, et al. A phase I combination study of olaparib with cisplatin and gemcitabine in adults with solid tumors. Clinical Cancer Research. 2012; 18:2344–2351. [PubMed: 22371451]

Robinson MD, Speed TP. A comparison of Affymetrix gene expression arrays. BMC Bioinformatics. 2007; 8:449. [PubMed: 18005448]

Sandhu SK, Schelman WR, Wilding G, Moreno V, Baird RD, Miranda S, Hylands L, Riisnaes R, Forster M, Omlin A, et al. The poly(ADP-ribose) polymerase inhibitor niraparib (MK4827) in BRCA mutation carriers and patients with sporadic cancer: a phase 1 dose-escalation trial. The Lancet Oncology. 2013; 14:882–892. [PubMed: 23810788]

Siegel D, Franklin WA, Ross D. Immunohistochemical detection of NAD(P)H:quinone oxidoreductase in human lung and lung tumors. Clinical Cancer Research. 1998; 4:2065–2070. [PubMed: 9748120]

Siegel D, Ross D. Immunodetection of NAD(P)H:quinone oxidoreductase 1 (NQO1) in human tissues. Free Radical Biology & Medicine. 2000; 29:246–253. [PubMed: 11035253]

Skoulidis F, Byers LA, Diao L, Papadimitrakopoulou VA, Tong P, Izzo J, Behrens C, Kadara H, Parra ER, Canales JR, et al. Co-occurring genomic alterations define major subsets of KRAS-mutant lung adenocarcinoma with distinct biology, immune profiles, and therapeutic vulnerabilities. Cancer Discov. 2015; 5:860–877. [PubMed: 26069186]

Tagliarino C, Pink JJ, Dubyak GR, Nieminen AL, Boothman DA. Calcium is a key signaling molecule in beta-lapachone-mediated cell death. J Biological Chemistry. 2001; 276:19150–19159.

Underhill C, Toulmonde M, Bonnefoi H. A review of PARP inhibitors: from bench to bedside. Annals of Oncology. 2011; 22:268–279. [PubMed: 20643861]

Wang M, Wu W, Wu W, Rosidi B, Zhang L, Wang H, Iliakis G. PARP-1 and Ku compete for repair of DNA double strand breaks by distinct NHEJ pathways. Nucleic Acids Research. 2006; 34:6170–6182. [PubMed: 17088286]

Wickham H. ggplot2: elegant graphics for data analysis: Springer Science & Business Media). 2009

Significance

Inhibitors of poly(ADP-ribose) polymerase (PARP) activity, similar to other DNA repair blockers, lack tumor-selectivity, are typically toxic to normal tissue and are only efficacious against a small subset of vulnerable (e.g., BRCA1/2 deficient) cancers by synthetic lethality. We show that the NAD(P)H:quinone oxidoreductase 1 (NQO1) bioactivatable drug, β-lapachone (ARQ761, ArQule, Woburn, MA, in clinical form), capitalizes on elevated *NQO1:CAT* ratios in recalcitrant pancreatic, non-small cell lung (NSCLC) and breast cancers to elicit tumor-selective programmed necrosis. Cells are killed independent of oncogenic driver or passenger mutations. β-Lapachone can be utilized to greatly expand the use of PARP inhibitors to synergistically and efficaciously kill solid tumors that overexpress NQO1.

Highlights

- Solid cancers overexpress NQO1, with low Catalase levels, reverse of normal tissue.
- β-Lapachone kills independent of oncogenic driver or passenger mutations.
- Synergy with PARP inhibitors and β-lapachone is NQO1-dependent.
- PARP inhibitors + β-lap induce DNA lesions, block repair, and cause apoptosis.

In Brief

Huang et al. show that combination treatment with NQO1 bioactivatible β-lapachone and a PARP inhibitor causes unrepaired DNA damage and induces apoptosis and that the combination treatment has a synergistic therapeutic effect in orthotopic pancreatic and non-small cell lung cancer models.

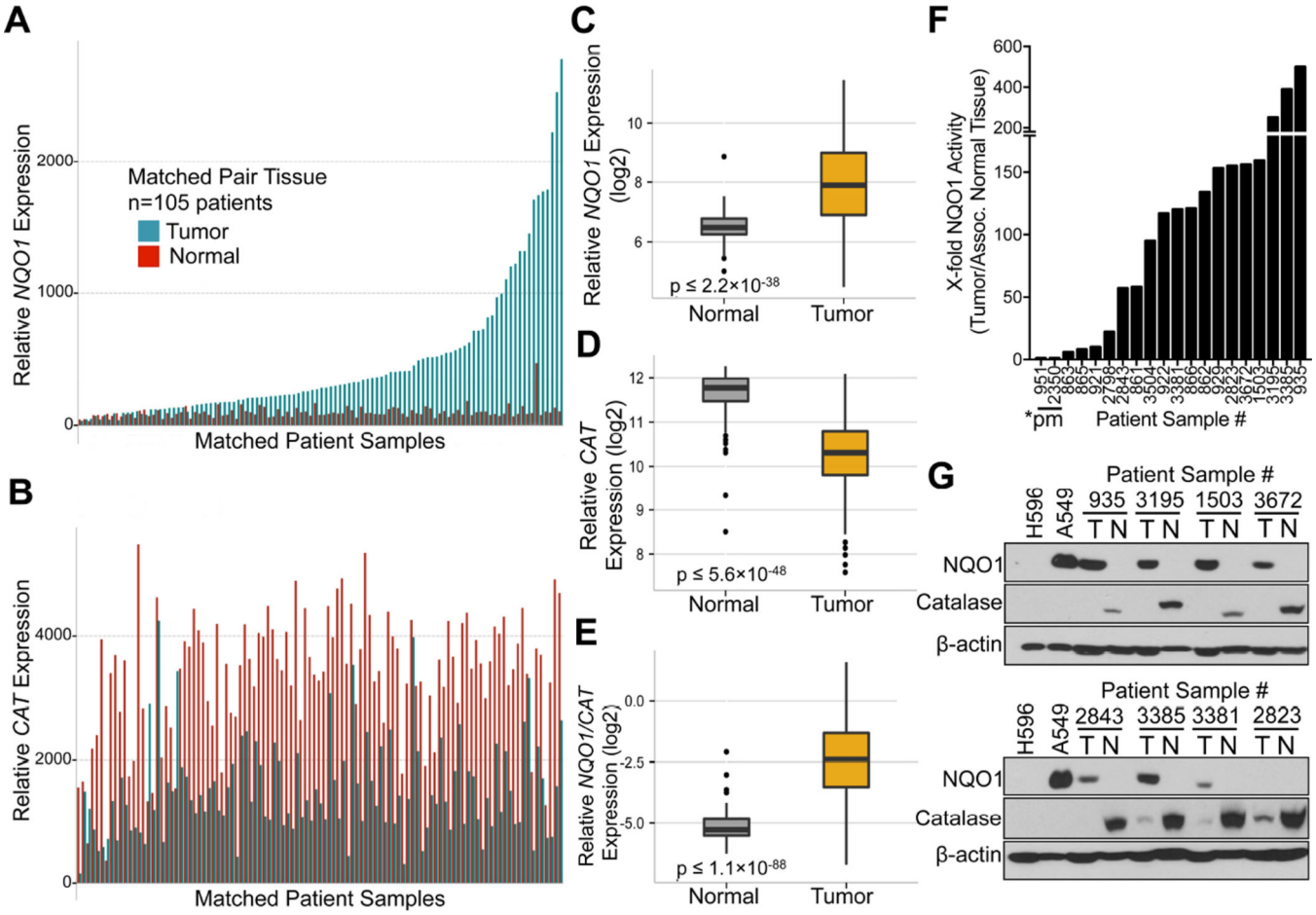

Figure 1. *NQO1* and catalase (*CAT*) expression in NSCLC tumor vs normal tissue

(A,B) mRNA expression data from matched NSCLC tumor and associated normal lung tissue (n=105) for: *NQO1* **(A)** and *CAT* expression **(B)**.

(C–G) NSCLC tumor (n=327) and associated normal lung (n=105) patient samples were analyzed for mRNA expression differences in *NQO1* ($p \leq 2.2 \times 10^{-38}$) **(C)**; *CAT* ($p \leq 5.6 \times 10^{-48}$) **(D)**, and calculated *NQO1/CAT* ratios ($p \leq 1.1 \times 10^{-88}$) **(E)**. NQO1 enzyme activities **(F)**: cytoC reduced/min/μg protein from fresh, snap-frozen patient NSCLC tumor tissue. *pm, *2 homozygous *NQO1* polymorphism tumors with no enzyme expression. Steady state *NQO1* and *CAT* protein levels were monitored from pathology-dissected de-identified patient NSCLC tumor (**T**) or associated normal (**N**) tissue by Western analyses **(G)**. Box Plots show patient sample data for *NQO1, CAT* and *NQO1/CAT* ratios with lines representing means ± SD.

See also Figure S1.

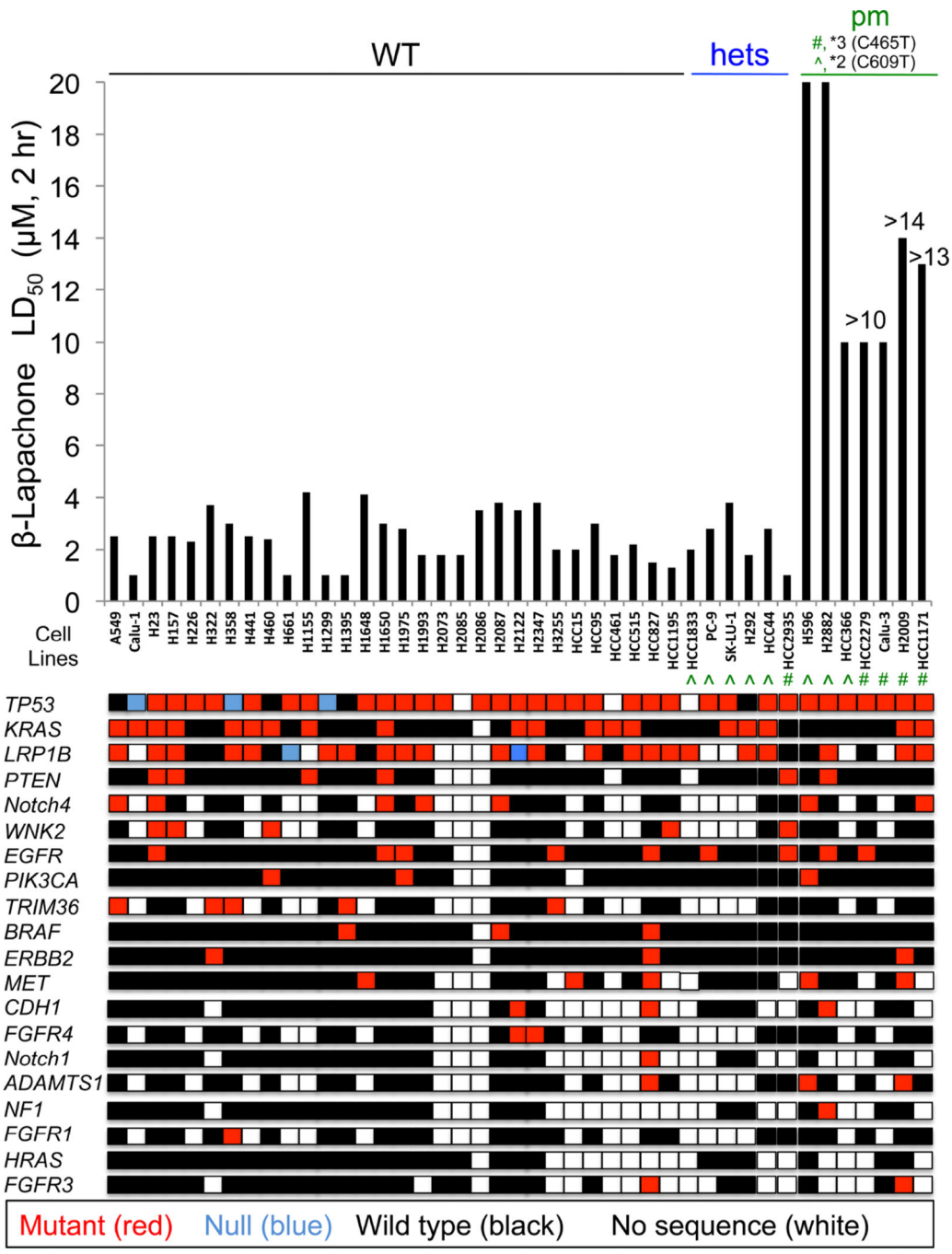

Figure 2. β-Lapachone lethality is dependent on *NQO1* status, but not oncogenic driver or passenger mutations

NSCLC cell lines were screened in a double-blind manner for lethality (LD_{50} values), *NQO1* polymorphism (Kolesar et al., 1995) and oncogene mutational statuses. *NQO1* polymorphic statuses were: WT (wild-type); hets (WT + polymorphic alleles: ^, *2 (C609T) or #, *3 (C465T), HCC2935); or pm, homozygous polymorphic (*2 or *3) alleles. Relative β-lap sensitivities were expressed as LD_{50} values (μM, 2 hr). Values with 'greater than (>)' signs indicate highest concentrations (μM) tested. DNA from NSCLC cells were sequenced

by the UTSW-MDA lung cancer SPORE (red: mutant, blue: null (deletion), black: wild-type, white: no sequence available).
See also Figure S2.

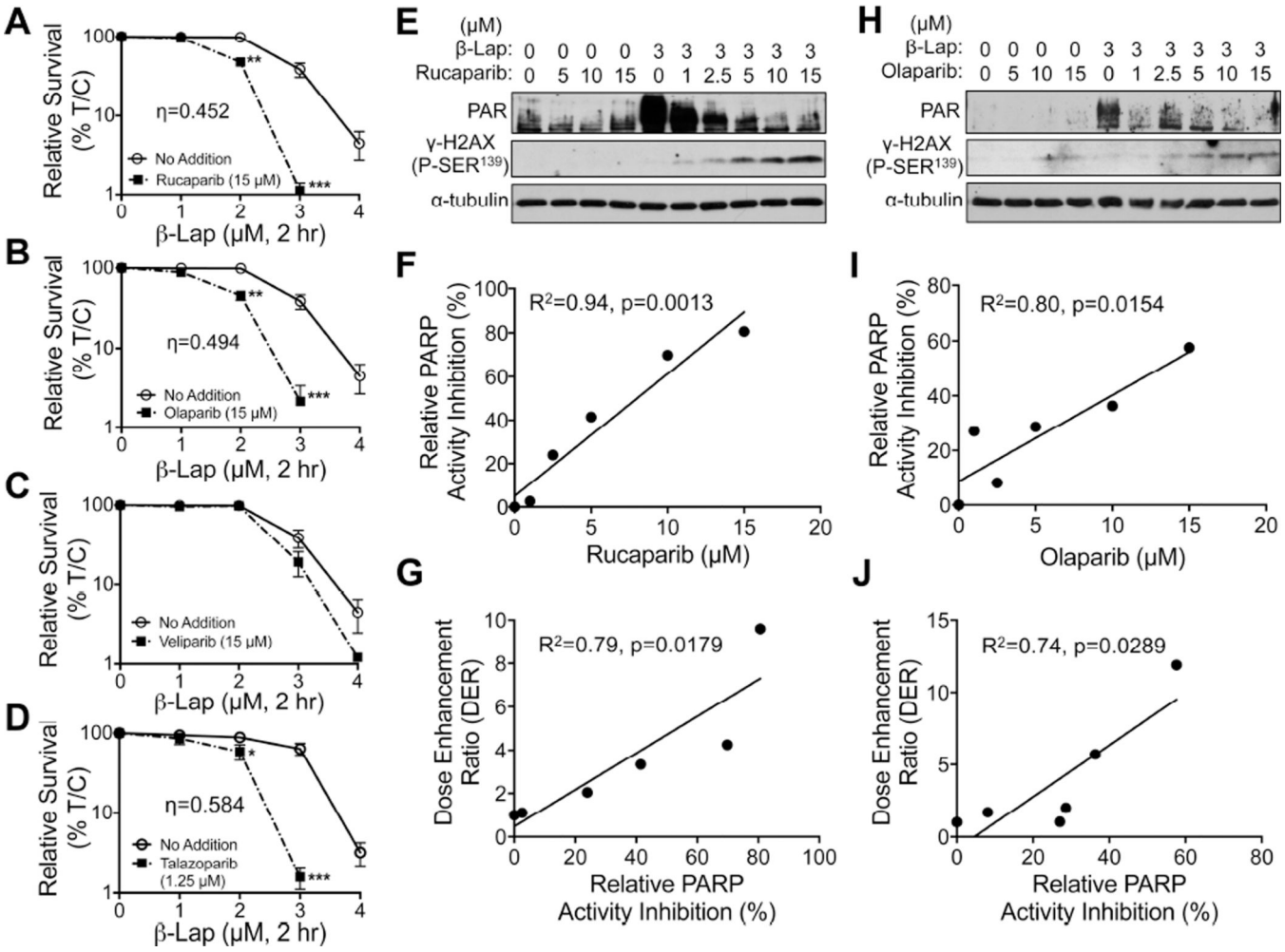

Figure 3. Synergy between nontoxic doses of PARP inhibitors and sublethal β-lapachone doses

(A–D) A549 NSCLC cells were pretreated for 2 hr with: Rucaparib **(A)**, Olaparib **(B)**, Veliparib **(C)**, each at 15 μM, or Talazoparib at 1.25 μM **(D)**, based on their relative toxicities alone (Figures S3A–S3D) followed by a 2 hr treatment with PARP inhibitor + various β-lap doses (Figures S3H–3K). Drugs were removed and survival assessed. All error bars are means ±SEM. ***, $p < 0.001$; **, $p < 0.01$; *, $p < 0.05$ (t tests). Synergy was calculated as per (Chou and Talalay, 1984). Synergy values for Rucaparib (η=0.452, p value=0.003), (Olaparib (η=0.494, p value=0.0013) and Talazoparib (η=0.548, p value=0.036) were reported based on multiple dose-responses, or on comparative p values indicated. **(E, H)** PAR and γH2AX formation alterations for DMSO or β-lap (3 μM)-exposed A549 cells treated with various doses of Rucaparib **(E)** or Olaparib **(H)**.

(F, I, G, J) Relative PARP activity inhibition for doses of Rucaparib **(F)** or Olaparib **(I)** and dose enhancement ratio (DER) correlations for Rucaparib **(G)** or Olaparib **(J)** dose-responses when combined with β-lap (3 μM).

See also Figure S3.

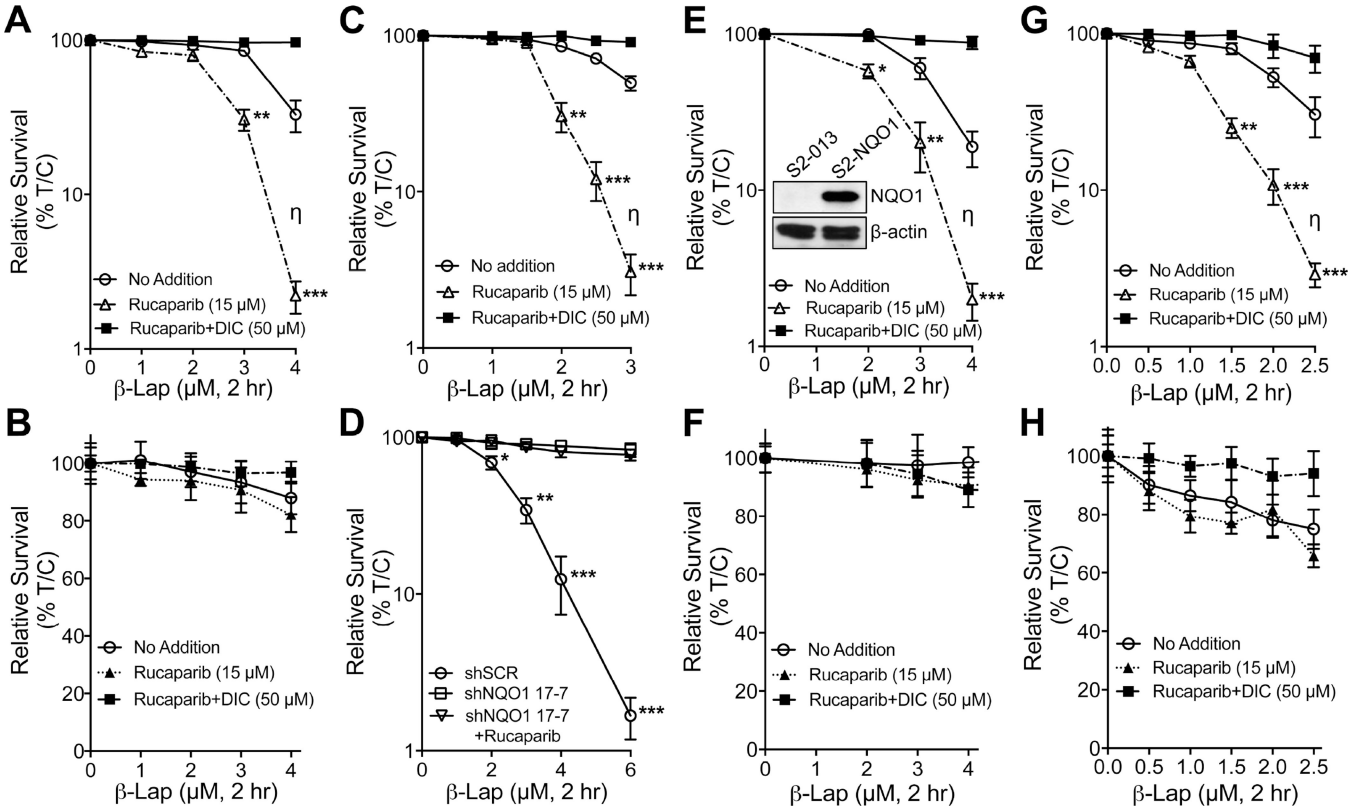

Figure 4. PARP inhibition and β-lapachone synergy is NQO1-dependent and broadly applied to various types of NQO1 over-expressing cancers

(A,B) Polymorphic *2 H596 NSCLC cells corrected for NQO1 expression **(A)** were pretreated with Rucaparib (15 μM, 2 hr) and then exposed or not to Rucaparib (15 μM) + β-lap (0–4 μM) for 2 hr. Cells were also exposed to β-lap, ± dicoumarol (DIC, 50 μM) for 2 hr and survival assessed. Genetically matched NQO1-deficient H596 NSCLC cells **(B)** were treated as in **(A)**, and survival assessed.

(C,D) *NQO1*$^{+}$ MiaPaCa2 PDA cells **(C)** were pretreated with Rucaparib (15 μM, 2 hr), then exposed or not to Rucaparib (15 μM) + β-lap (0–3 μM or 0–6 μM for **D**, respectively) for 2 hr, ± dicoumarol (DIC, 50 μM). Drugs were removed and survival assessed. Stable shRNA-*NQO1* down MiaPaCa2 (clone 17–7) vs shSCR MiaPaCa2 cells **(D)** were treated as in **(C)**, but without dicoumarol and assessed for survival.

(E,F) *NQO1*$^{+}$ Suit2 (S2-013) PDA cells **(E)** harboring a *CMV-NQO1* over-expression vector (see Western, inset) were pretreated with Rucaparib (15 μM) and then exposed or not to β-lap (0–4 μM), ± dicoumarol (DIC, 50 μM) for 2 hr. Genetically matched, *NQO1*$^{-}$ *2 polymorphic S2-013 chemo- and radio-resistant PDA cells **(F)** expressing shSCR were treated as in **(E)** and survival assessed. See inset **(E)** for NQO1 expression. **(G,H)** MDA-MB-231 *2 polymorphic TNBC cells corrected for NQO1 expression **(G)** were pretreated with Rucaparib (15 μM, 2 hr), + β-lap (0–2.5 μM), ± dicoumarol (DIC, 50 μM) for 2 hr. Drugs were removed and survival assessed. shSCR *NQO1*$^{-}$ MDA-MB-231 TNBC cells **(H)** lacking NQO1 expression were treated as in **(G)** and assessed for survival. (**A–H**) was evaluated as described (Chou and Talalay, 1984). Synergy values (η=0.452, p value=0.0003) were reported based on multiple dose-responses, or on comparative p values indicated.

All error bars are means of six replicates from three independent experiments; means ± SEM. ***, $p < 0.001$; **, $p < 0.01$; *, $p < 0.05$, comparing each data point to those of single treatments (t tests).

See also Figure S4A–S4D.

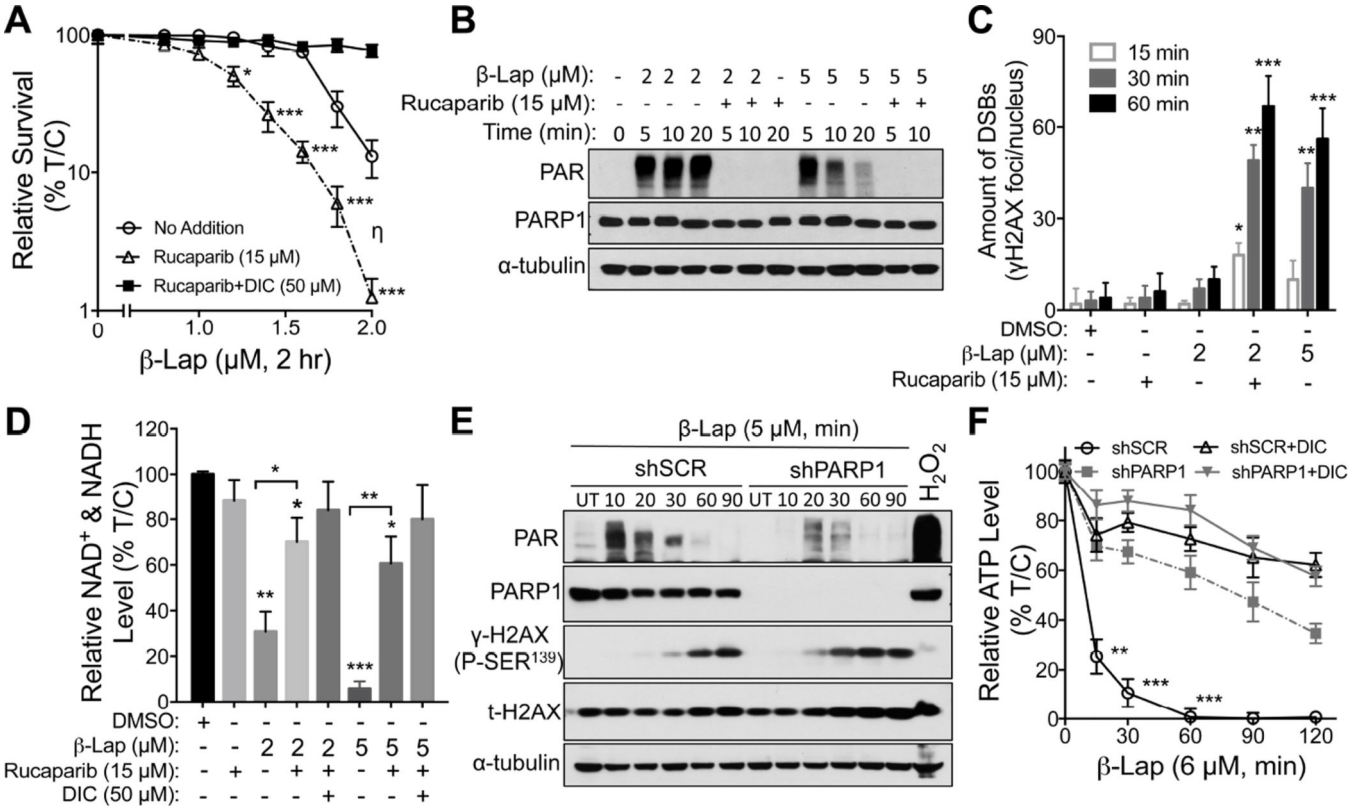

Figure 5. PARP inhibition in MCF-7 breast cancer cells confers hypersensitivity to sublethal β-lapachone doses

(A–D) MCF-7 cells were pretreated ± Rucaparib (15 μM, 2 hr), then exposed or not to Rucaparib (15 μM) + β-lap (0–2.0 μM) for 2 hr. Cells were also exposed to β-lap, ± dicoumarol (DIC, 50 μM) for 2 hr, and survival assessed **(A)**. Synergistic lethality between β-zlap and Rucaparib (η) was determined as in Figure 3. MCF-7 cells were pretreated ± Rucaparib (15 μM, 2 hr), then ± Rucaparib (15 μM) or two different doses of β-lap (2.0 or 5.0 μM) for 2 hr, ± dicoumarol (DIC, 50 μM). Levels of PAR (PARP hyperactivation) formation were assessed with α-tubulin as loading controls **(B)**. Cells from **(B)** were assessed for DSBs by γH2AX foci/nuclei **(C)** and for relative NAD^+ & NADH levels **(D)**. Synergy values (η=0.452, p value=0.0003) were reported based on multiple dose-responses, or on comparative p values indicated.

(E) Stable shSCR or shPARP1 knockdown MCF-7 breast cancer cells were exposed or not to β-lap (5 μM) and cell extracts prepared at indicated times (up to 90 min). shSCR MCF-7 cells were also exposed to H_2O_2 (500 μM, 15 min). Westerns confirmed PARP1 knockdown, and PAR and γH2AX formation. Protein loading was confirmed by total H2AX (t-H2AX) and α-tubulin levels.

(F) Changes in relative ATP levels were measured in DMSO- or β-lap (6 μM)-treated stable shSCR or shPARP1 knockdown MCF-7 cells at indicated times (min), ± dicoumarol (DIC, 50 μM).

All error bars are means ± SEM from three independent experiments. ***, $p < 0.001$; **, $p < 0.01$; *, $p < 0.05$ (t tests).

See also Figures S4E–S4J.

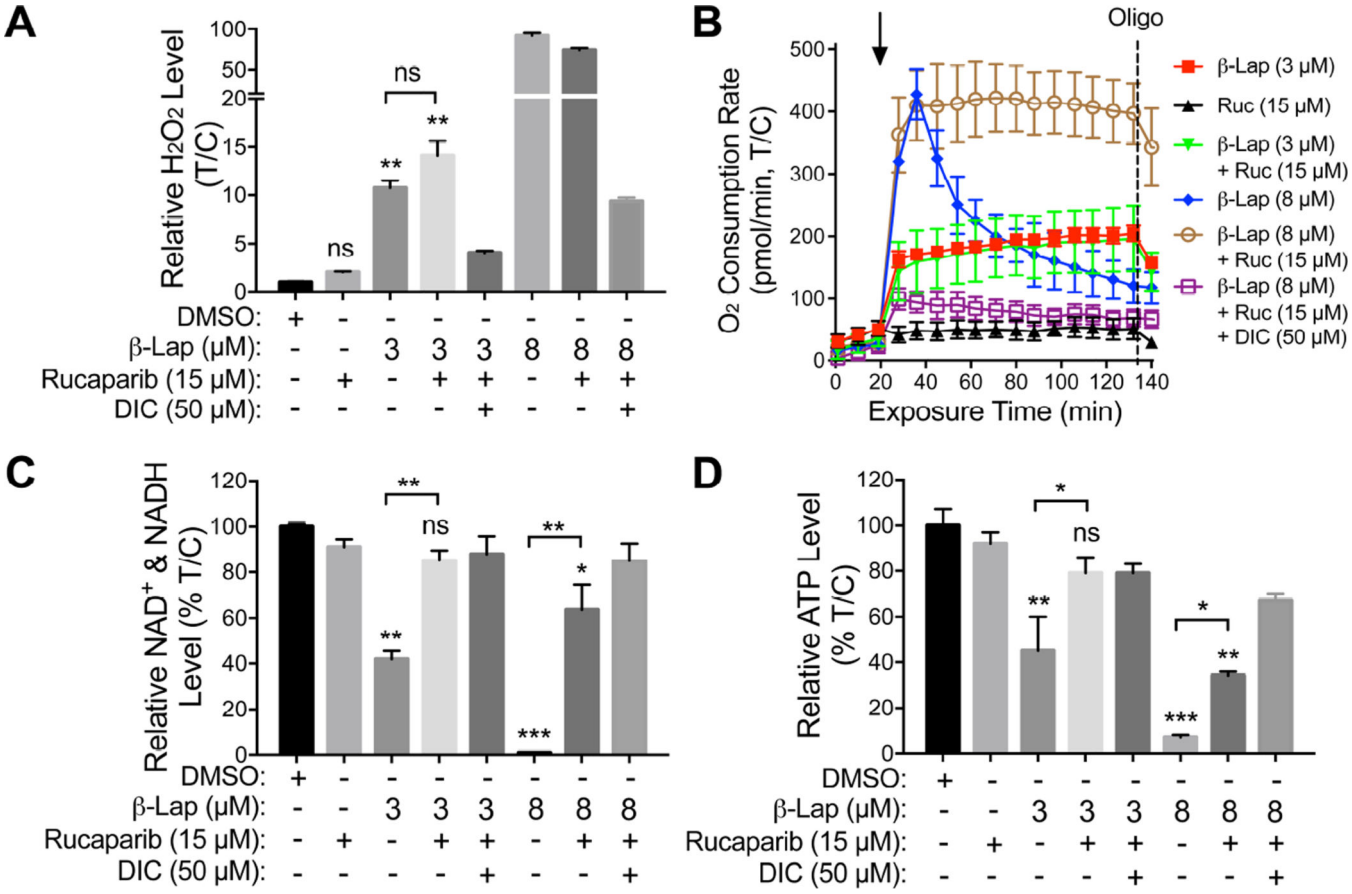

Figure 6. Inhibition of β-lapachone-stimulated, NQO1-dependent PARP1 hyperactivation by Rucaparib spares catastrophic energy loss

(A–D) *NQO1*$^+$ A549 NSCLC cells were pretreated with Rucaparib (15 μM, 2 hr), then exposed or not to Rucaparib (15 μM) + β-lap (3 or 8 μM), ± dicoumarol (DIC, 50 μM) for 2 hr. Cells were also treated with β-lap (3 or 8 μM, 2 hr) alone. Cells were then monitored for: Long-term ROS formation (i.e., relative H_2O_2 levels) at 2 hr **(A)**; Real-time oxygen consumption rates (OCRs) after various drug treatments (added at t=20 min, arrow) by Seahorse XF analyses: Ruc, Rucaparib; Oligo, oligomycin **(B)**; Total NAD^+ and NADH levels **(C)**; and Relative ATP levels after 2 hr treatments (**D**). Results were separately repeated at least three times in triplicate each. Results (means ± SEM) from three independent experiments. ***, $p < 0.001$; **, $p < 0.01$; *, $p < 0.05$ (t tests).

See also Figures S5A–S5D.

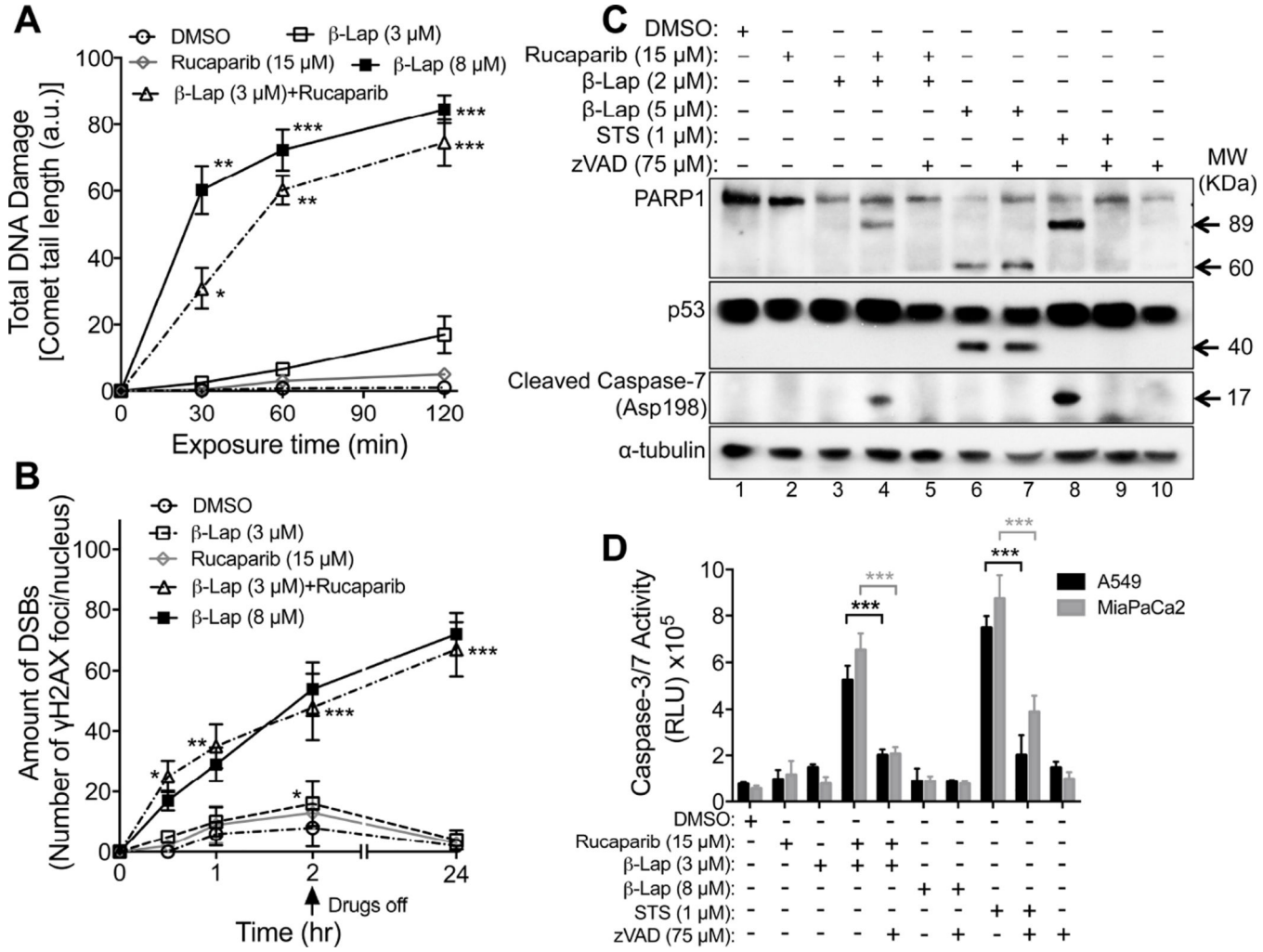

Figure 7. PARP inhibitors prevent DNA repair, increase DSB formation, and switch cell death pathways in β-lapachone-exposed *NQO1*$^+$ cancer cells

(A,B) *NQO1*$^+$ A549 NSCLC cells were treated with Rucaparib alone, β-lap alone and/or Rucaparib + β-lap under conditions outlined in Figure 6. Cells were assessed for: Total DNA lesions using alkaline comet assays **(A)**. Comet tail-lengths in arbitrary units (a.u.) were monitored at various times (min); and DSBs quantified by γH2AX foci/nuclei using immunofluorescence at indicated times (hr, hours) **(B)**. Sublethal (3 μM) and lethal (8 μM) β-lap doses were used. Arrow indicates drug removal.

(C)*NQO1*$^+$ MCF-7 cells were pretreated ± Rucaparib (15 μM, 2h), then exposed or not to Rucaparib (15 μM) + β-lap (2 μM), ± zVAD-fmk (pan-caspase inhibitor, 75 μM) for 2 hr. Cells were also exposed to Staurosporine (STS, 1 μM, 18 hr) or β-lap (5 μM, 2 hr), ± zVAD-fmk (75 μM) to detect apoptotic or programmed necrotic (NAD$^+$-Keresis) death pathways. After 24 hr, proteolytic markers of cell death were assessed, including PARP1 (89 kDa for apoptosis, ~60 kDa for programmed necrosis), p53 (~40 kDa for programmed necrosis) or caspase 7 (apoptosis) cleavage, or α-tubulin for loading control.

(D)*NQO1*$^+$ A549 NSCLC or MiaPaCa2 PDA cells were pretreated ± Rucaparib (15 μM, 2 hr), then ± Rucaparib (15 μM) + β-lap (3 or 8 μM), ± zVAD-fmk (75 μM) for 2 hr. Cells

were also exposed to DMSO, β-lap (3 or 8 μM, 2 hr) or Staurosporine (STS, 1 μM, 18 hr), ± zVAD-fmk and monitored for caspase 3/7 activation after 48 hr. Graphed are means ± SEM from three experiments in A, B and D. Student's t tests were performed. ***, $p < 0.001$; **, $p < 0.01$; *, $p < 0.05$.

See also Figure S5E.

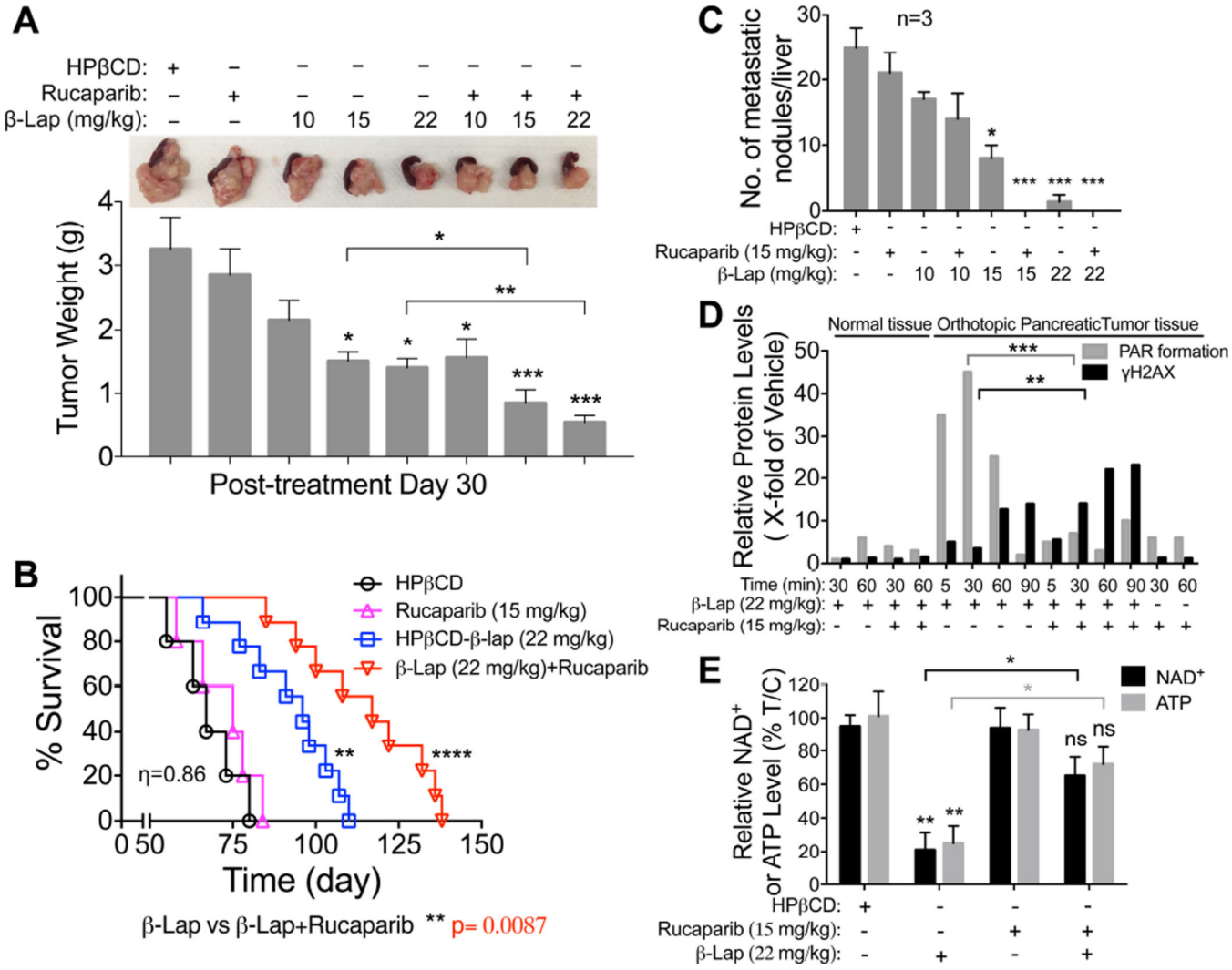

Figure 8. PARP inhibitors synergize with β-lapachone against orthotopic MiaPaCa2 PDA xenografts

(A, B) Orthotopic MiaPaCa2 tumors were established in 20–22 g female NOD/SCID mice by injecting ~1 X 10^6 cells into the pancreas. After 3 weeks, mice were treated or not with Rucaparib (15 mg/kg, ip) and after 2 hr with vehicle (HPβCD, iv) or HPβCD-β-lap (22 mg/kg, iv) by tail vein injections every day for 5 injections. Mice recovered seven days, followed by another five daily injections. Representative mouse tumors at day 30 post-treatment, with averages ± standard error of tumor volumes per treatment condition (n=3) **(A)**, Kaplan-Meier survival curves **(B)**. ****, $p < 0.0001$; **, $p < 0.01$, β-lap (22 mg/kg) or combined treatment vs HPβCD alone treatment (log-rank test). Synergy values (η=0.86) were reported based on multiple dose-responses, or on comparative p values indicated.

(C) Assessment of metastatic tumor nodules in livers of mice at day 30 post-treatment.

(D) Orthotopic MiaPaCa2 pancreatic tumor-bearing female NOD/SCID mice (3/group) were treated as in **(A)** and sacrificed at indicated times (min). Blood, tumor and various normal tissues (including associated normal pancreas) were extracted and analyzed for drug levels

and PAR-PARP and γH2AX formation with β-actin loading. Experiments were repeated three times.

(E) Tumor tissues from **(D)** were assessed for NAD^+ or ATP pools at 90 min post exposure. Graphed are means ± SEM from three mice in each group in A, C, D and E. Student's t tests were performed. ***, $p < 0.001$; **, $p < 0.01$; *, $p < 0.05$; ns, not significant.

See also Figures S6, S7